Physics of the Solid State, 2025, Vol. 67, No. 11

08,03,06

Depolarization currents in the $BiFeO_3/TiO_2$(Nt)Ti structure depending on the exposure time and the magnitude of the polarizing voltage

© G.M. Gajiev, Sh.M. Ramazanov¶, N.S. Abakarova, T.N. Efendieva

Amirkhanov Institute of Physics, Daghestan Federal Research Center, Russian Academy of Sciences, Makhachkala, Russia

¶ E-mail: ramazanv@mail.ru

Received September 15, 2025
Revised November 7, 2025
Accepted November 10, 2025

The behavior of depolarization currents in the $BiFeO_3/TiO_2$(Nt)Ti film structure after removing external voltage was studied as a function of the exposure duration (0−4 s) and voltage (30−55 V). An ambiguous relationship between the relaxation time and polarization time was established, caused by leakage currents and the processes of carrier trapping/emission to defect levels (oxygen vacancies) of the sample. Relaxation processes and leakage currents significantly determine the electrical properties of $BiFeO_3$-based memristor structures. Characteristic relaxation times and their relationship with the state of traps allow us to consider the depolarization current analysis technique as an effective tool for diagnosing the quality of films and assessing their operational limits.

Keywords: $BiFeO_3$, depolarization current, nanotubes, thin films, ferroelectric memristor.

DOI: 10.61011/PSS.2025.11.62964.252-25

1. Introduction

The needs for processing of large data volumes that grow year on year revealed a problem of lacking compute capacity in computers based on the von Neumann architecture. The achieved technological limit of the dimensions and response of classic microchips brings no hope to solve this problem. The solution to the problem was the initiation of the projects for the development of new generation processors, where the so called „von Neumann bottleneck effect“ is overcome by geometrical registration of the memory and the arithmetic-logic unit in a single chip [1,2]. The main component in this design is a memristor — a double-pole nonvolatile memory element, whose functionality is provided by the phenomenon of bistable resistive switching [3].

Among the thin-film oxides of transition metals seen as promising materials for memristor manufacturing, a semiconductor (dielectric) $BiFeO_3$ (BFO) plays a special part. BFO, apart from outstanding multiferroic properties — high values of temperatures of the magnetic $T_N = 370\,^\circ$C and segnetoelectric $T_c = 820\,^\circ$C ordering [4,5], previously also demonstrated pronounced properties of resistive switching [6,7]. Some papers show that, for enhancement of magnetoelectric effect, improvement of electrophysical and electrochemical properties of BFO-based films, buffer layers (in particular, array of TiO_2(Nt) nanotubes) may be used, which expands the range of applications of these materials [8–11].

Relaxation currents arising in thin-film segnetoelectrics immediately after voltage connection/disconnection provide substantial impact on the operation of the memory elements, depend strongly on the processes of polarization and depolarization, sometimes causing a noticeable modification of $J-V$ dependences [12–14]. The relaxation time defined from the dependence $J(t)$ after voltage supply/relief on the sample is an important parameter of active dielectrics. Its value depends on the extent of the material structure perfection, the presence of the current carrier shallow traps and the state of the interface of the film structure phases, and may reach the values from fractions of a second to several minutes. Therefore, the analysis of the curve $J(t)$ is a convenient tool to characterize the sample to identify the extreme conditions for the operation of the memory elements, at which the films degrade.

In the literature they often describe the PUND-method (positive up negative down) to evaluate the polarization losses in dielectrics, where after the pre-polarizing triangular voltage pulse (lasts for dozens of microseconds) after a time of delay of around 100 s the polarization loss is measured using a short triangular pulse [6,15,16]. There are very few papers where the relaxation current is studied immediately after the relief of voltage applied to the sample for several seconds, especially regarding the film structures.

In this paper we report the dynamics of the change in the depolarization currents in the film structure BFO-TiO_2(Nt)-Ti (BFOT) depending on the value of the pre-polarizing voltage (30−55 V) and duration of exposure thereto (0−4.0 s).

2. Samples and experimental procedure

BFO films were grown by atomic layer deposition (ALD) on ALDCERAM ML-200 unit. A titanium plate was used as a substrate, on which TiO_2(Nt) film in the form of vertical nanotubes was previously obtained by

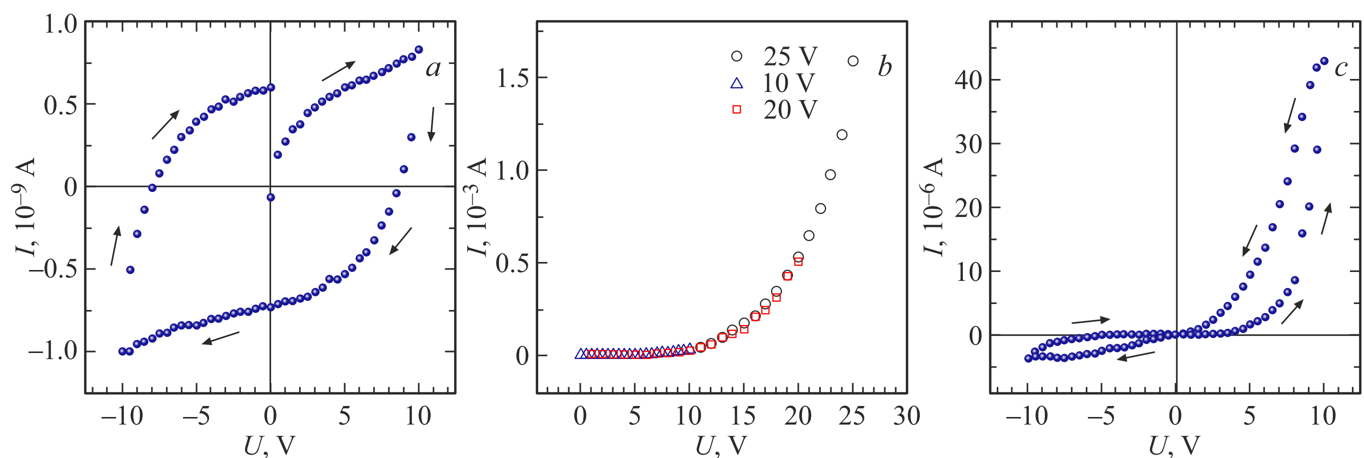

Figure 1. *a*) — VAC of the sample prior to electroforming with measurement delay of 0.1 s. *b*) — process of film electroforming with measurement delay of 1 s. Values of limit voltages in each VAC cycle are specified. *c*) — VAC after electroforming with delay time of 0.1 s.

electrochemical method. The thickness of TiO_2(Nt) layer was $\sim 2.5\,\mu$m. The BFO film thickness was ~ 90 nm, the evaluation was carried out using the method of transmission electron microscopy in the sample dent [10]. $Bi(mmp)_3$ and ferrocene $Fe(cp)_2$ were used as sources of precursors. The temperature range of $Bi(mmp)_3$ evaporation was 135–145 °C, the evaporation temperature of ferrocene was 90 °C. ALD BiO_x consisted of $Bi(mmp)_3$ precursor pulse with width of 1.2 s, then purging with N_2 admission of pulse of O_3 — 5 s, in the interval between cycles nitrogen purging was carried out for 15 s. Cycles of ALD FeO_x were then applied. The pulse width of $Fe(C_5H_5)_2$ precursor — 2 s. The number of admission subcycles of each precursor was 90. Throughout the entire experiment, the inlet and outlet gas pipelines were maintained at a temperature of 150 °C. The substrate was located at a distance of 4–5 cm from the inlet. The reactor was heated uniformly to 250 °C. Afterwards, the resulting samples were heat treated in air at temperature of 660 °C for 60 min. To carry out electrical measurements, the contacts were deposited on the surface using magnetron sputtering, and a titanium substrate served as the bottom electrode. The experimental part of the fabrication of this structure is described in more detail in paper [10].

Electrical measurements were performed on Keithley 2400 source-meter. Voltage of rectangular shape with duration from 100 ms to 4 s and amplitude in the interval of 30–55 V was applied to the sample, and after its relief the $J(t)$ was measured for several seconds. The operation of the source meter was automated in the LabVIEW environment. The upper electric contact was created by a press (spring) platinum electrode with diameter of 0.3 mm, the lower contact was a titanium substrate. Electric capacity of films at 100 Hz and 100 kHz was measured on an LCR-meter AKTAKOM AM-3001 at the voltage of the metering sinusoidal signal at 0.25 V.

3. Results and discussion

This section specifies the experimental data on the study of electrical properties of BFOT film structure. The primary attention is paid to VAC, electroforming processes and the dynamics of the depolarization currents after removal of the external polarizing voltage. The obtained dependences make it possible to identify the specific mechanisms of current flow, including the impact of Maxwell-Wagner polarization, formation and destruction of conducting filaments, and the processes of carriers capture and emission at deep levels. Comparison of the structure behavior at various times and values of applied voltage made it possible to establish the relationship between the polarization time, the amplitude of the initial relaxation current and leakage mechanisms, defining the electrical stability of the studied structures. Figure 1 presents the VAC of the BFOT film structure measured in the voltage sweep in the form of a bidirectional signal of triangular shape (Figure 1, *a, b*) and in linear sweep (Figure 1, *c*) with the increase of the voltage limit in every subsequent VAC cycle.

At each sweep point the measurement was carried out according to the following scheme: voltage generation — delay (waiting) — current measurement [17]. The presence of the VAC hysteresis loop in high-resistance state (Figure 1, *a*) is due to the Maxwell-Wagner polarization (MWP), which consists in charge accumulation at the interface due to conductivity currents passing through a two-layer sample causing redistribution of electric fields and pressure drops in the layers [18]. The process ends at $t \gg \tau$ (MWP relaxation time), when only a through component of conductivity remains. After disconnection of external voltage, depolarization is observed. The times of polarization and depolarization are usually equal [18]. As a result of MWP an internal field arises in the sample that is directed towards the external one, when the current through the structure in voltage sweep is determined by the

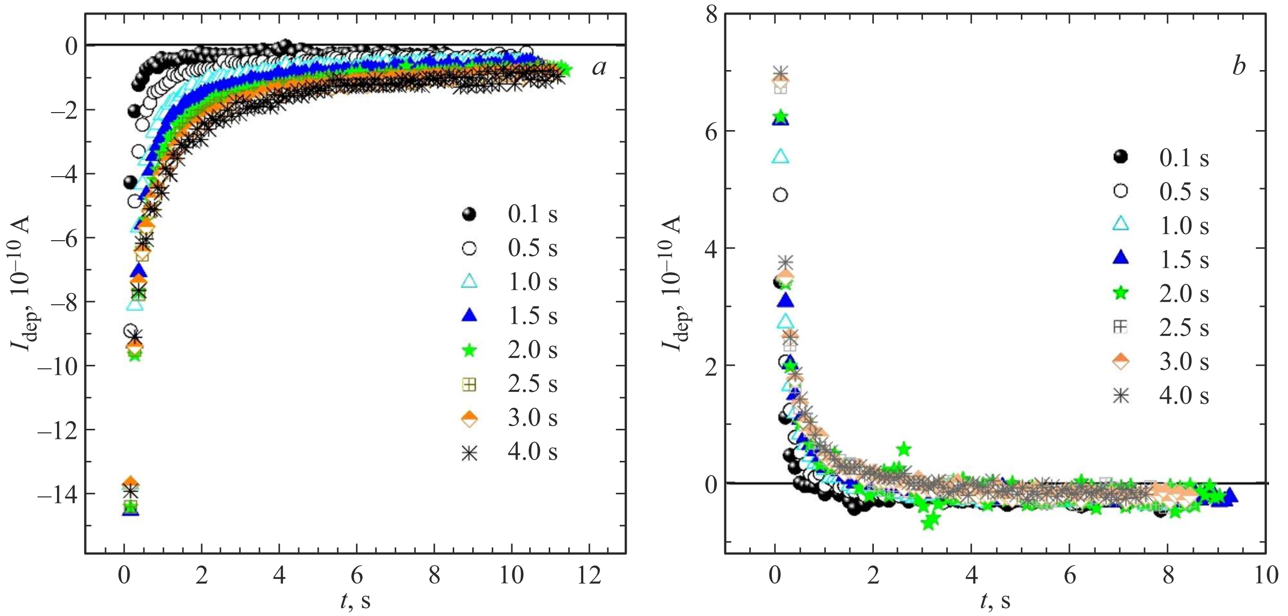

Figure 2. Depolarization current relaxation curves after external voltage relief to zero, *a*) — $U_{pol} = 55$ V; *b*) — $U_{pol} = -55$ V. Figures on the right show the times of delay of the polarizing voltage on the sample.

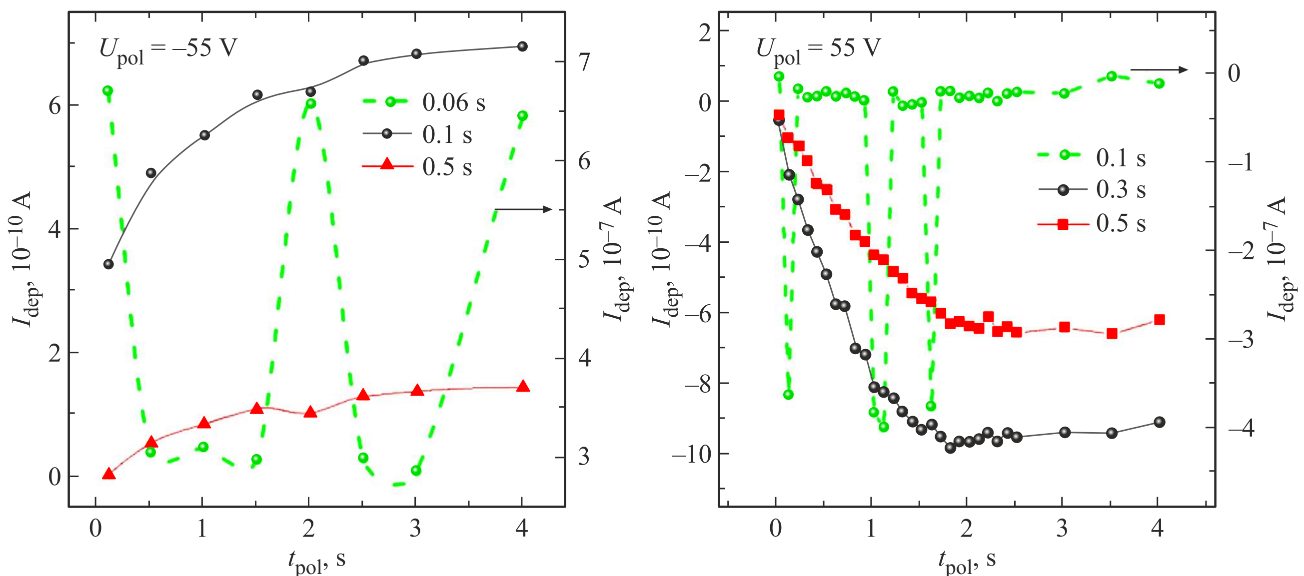

Figure 3. Impact of time of polarizing voltage application (values specified on top to the left) on depolarization currents read within times (specified near symbols) after voltage disconnection.

following ratio [18]:

$$I = \frac{V - V_P}{R_0}, \quad (1)$$

where V — external voltage; V_P — voltage corresponding to the internal field; R_0 — sample resistance.

Electroforming of the sample (Figure 1, *b*) means formation of current-conducting threads (filaments) at high values of electric field. Sample VAC after electroforming (Figure 1, *c*) demonstrates the effect of resistive switching that happens in formation or destruction of current-conducting threads in a dielectric. Formation of filaments is related to the redistribution of oxygen vacancies that arise unavoidably in process of annealing at a certain process stage of sample manufacturing, when the external electric field is applied. A chain of positively charged oxygen vacancies arises along the field. Accumulation of oxygen vacancies at the boundary of heterojunction and in the field of electrode-film contact causes a change in the width and height of the corresponding energy barriers, which in the

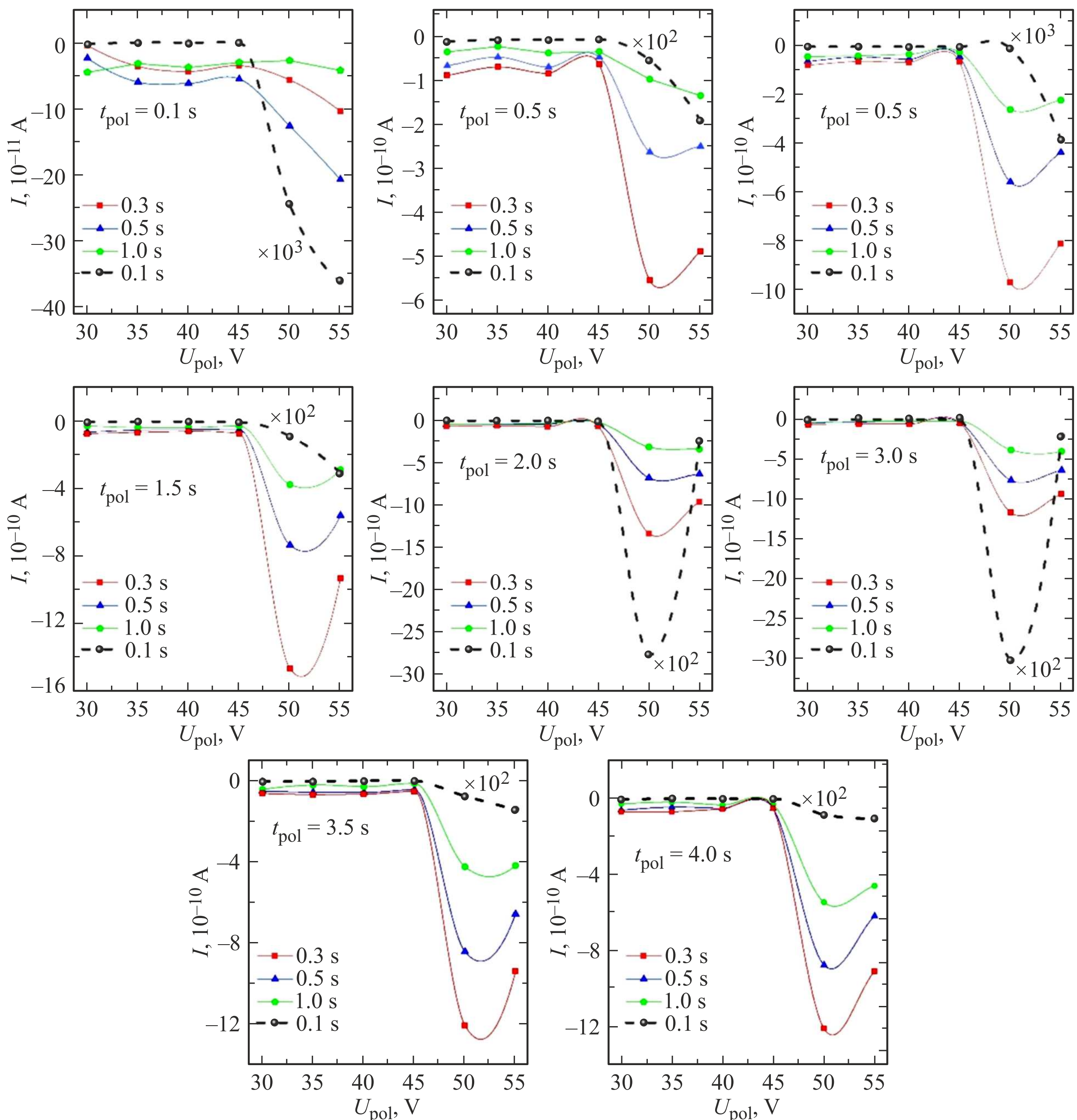

Figure 4. Dynamics of depolarization currents variation with increase of polarizing voltage exposure time and its value at various moments of time (specified below at the bottom in the boxes) after voltage disconnection.

end affects the resistance of the sample [19]. We relate a diode-like VAC in Figure 1, *c* to the heterojunction at the phase boundary of the film structure. Figure 2 shows the relaxation of the depolarization currents after disconnection of polarization voltage $U_{pol} = 55\,V$ (Figure 2, *a*) and $U_{pol} = -55\,V$ (Figure 2, *b*) applied to the sample for different periods of time — from 0.1 s to 4 s.

From Figure 2 you can see that as time of polarization voltage waiting increases, the initial depolarization current in the sample increases, and the curvature center $I_{dep}(t)$ slightly moves along the time axis to the right. Graphically this process is shown in Figure 3, which provides dependences of depolarization currents on time of external voltage application to the sample $I_{dep}(t_{pol})$ measured at different time after resetting the voltages shown in the figure.

Curves $I_{dep}(t_{pol})$ measured in 0.1 s and 0.5 s after resetting voltages $U_{pol} = -55\,V$, $U_{pol} = 55\,V$ (Figure 3.) demonstrate a weak growth reaching saturation, which logically presumes increase of the MWP degree with the increasing polarization time. As for the curves $I_{dep}(t_{pol})$ at the early stages of relaxation (0.06 s for $U_{pol} = -55\,V$ and 0.1 s for $U_{pol} = 55\,V$), the curves contain ambiguities. The

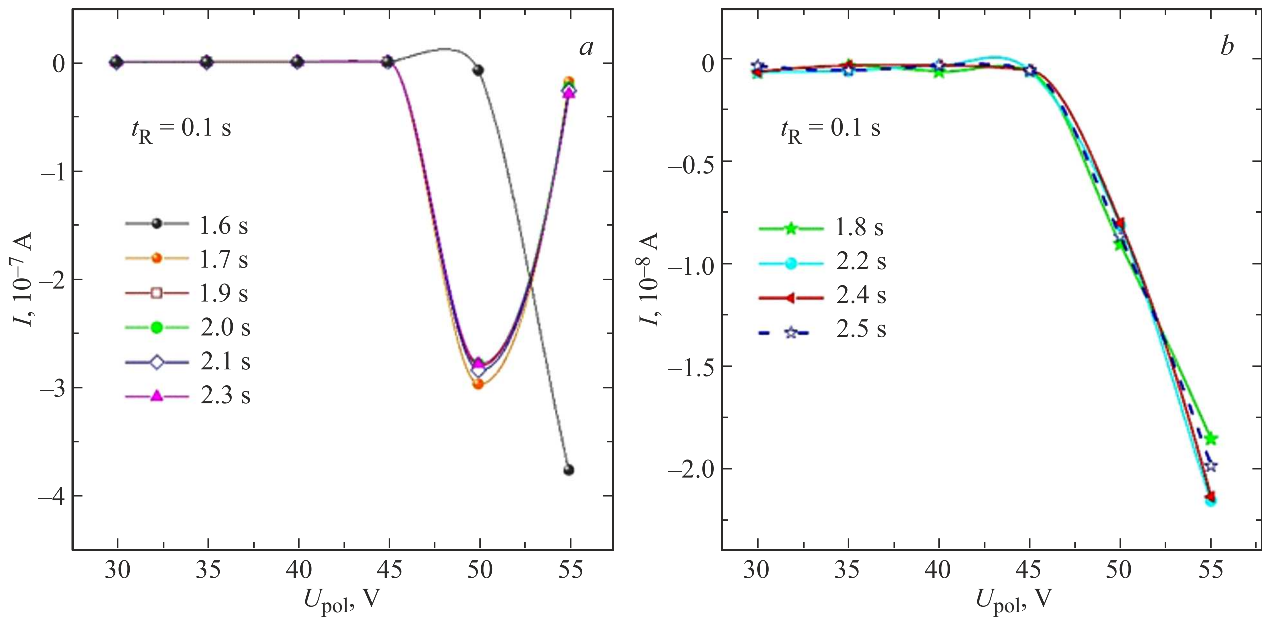

Figure 5. Behavior of depolarization currents in the sample exposed to the polarization voltage for different periods of time (specified near symbols) measured in 0,1 sec after voltage is reset.

dependence $I_{dep}(t_{pol})$ for the current reading time of 0.06 sec after disconnection of $U_{pol} = -55$ V has clear maxima with the polarization time period of 2 s, but at the same time every 0.5 s there is current drop or rise observed. In case of $U_{pol} = 55$ V, though there is no strict periodicity for current surges in curve $I_{dep}(t_{pol})$ for 0.1 s reading time, there is a weak correlation with periodicity of ~ 0.5 s in the field of ~ 0 — 2 s. You can say that the polarization times multiple to ~ 0.5 s at the initial stage of current relaxation are specific values.

Such features of depolarization currents at the initial moment of relaxation time are interpreted by us as the result of influence of charge carrier capture/depletion processes at the deep levels with time called the time of deep level filling relaxation [20]. Deep levels in our samples may be oxygen vacancies. In our previous paper [17] it was shown that time ~ 0.5 s is a specific value for transition currents after energizing the sample. Therefore, you can assume with a great degree of probability that at polarization times ~ 0.5 s and times multiple to this value, polarization and, accordingly, depolarization are modulated. Consolidated information on the dynamics of depolarization currents change with variation of the time of polarizing voltage application and its value read at different initial times after resetting the external voltage $I(U_{pol})$ to zero for the reading time of 0.3, 0.5 and 1 s passes through the maximum (using absolute value) in the vicinity of voltage ~ 50 V starting from the polarization time of $t_{pol} = 0.5$ s and to $t_{pol} = 4$ s (see Figure 4).

The current value in the maxima is the lowest with the longest reading time t_R after the voltage is reset to zero as should happen according to Figure 2. The nature of curves $I(U_{pol})$ for the reading time 0.1 s stands out of the general picture. Maxima $I(U_{pol})$ are only observed for $t_{pol} = 2$ s and $t_{pol} = 3$ s. In more detail the section between these polarization time values is considered in Figure 5, where you can see that maxima at dependences $I(U_{pol})$ manifest themselves at polarization time between 1.7 and 2.3 s (Figure 5, *a*), and further the non-monotonic growth of current occurs (Figure 5, *b*).

Maxima in Figure 4 and Figure 5 are the consequences of polarization loss at these periods of time when voltage above 50 V was active as a result of leakage currents caused by different mechanisms. In the field of high fields (> 20 kV/cm, Figure 1, *b*) the presence of current flow mechanisms was analyzed, being initiated by Schottky, Poole-Frenkel emissions and space charge limited current (SCLC). VAC (Figure 1, *b*) was rearranged in Schottky (Sch) $\ln(I) - E^{1/2}$, Poole-Frenkel (P-F) $\ln(I/E) - E^{1/2}$ and SCLC $\ln(I) - \ln(E)$ coordinates. Sections of these dependences have linear nature in the field of high intensities (> 20 kV/cm). Inclination coefficients K_{Sch}, $K_{P\text{-}F}$ and K_{SCLC} of the corresponding straight lines were defined for them. In SCLC coordinates the value K_{SCLC} turned out to be higher than 4, i.e. this mechanism in this area is not acceptable. Using K_{Sch} and $K_{P\text{-}F}$ coefficients, the values of dielectric constant were read using formula [21]:

$$\varepsilon_i = \frac{1}{(kT)^2} \frac{q^3}{m\pi\varepsilon_0} \frac{1}{K^2}, \qquad (2)$$

where coefficient m for Schottky mechanism is equal to 4, and for Poole-Frenkel mechanism — 1, K — inclination coefficient corresponding to values m, ε_0 — electric constant. The calculations showed that Poole-Frenkel emission was

the main mechanism of leakage currents in the area of high fields: $\varepsilon_i \approx 2.2$ for $K_{P\text{-}F} = 0.02$.

4. Conclusion

As a result of completed studies it was found that as the polarization time increases, the initial depolarization current amplitude grows. Specific relaxation times (~ 0.5 s) indicate the influence of charge carrier capture/emission processes on the oxygen vacancies. Poole-Frenkel emission is the main mechanism of leakage currents in the area of high fields: $\varepsilon_i \approx 2.2$ for $K_{P\text{-}F} = 0.02$, at voltages of around 50 V. The obtained results show that the relaxation processes substantially define the behavior of memristive structures based on $BiFeO_3$. The method to analyze the depolarization currents may be used to diagnose the quality of films and to predict the operational stability of new generation memory elements.

Conflict of interest

The authors declare that they have no conflict of interest.

References

[1] J. Borghetti, G.S. Snider, P.J. Kuekes, J.J. Yang, D.R. Stewart, R.S. Williams. Nature Letters **464**, 873 (2010).
[2] J. Yang, D.B. Strukov, D.R. Stewart. Nat. Nanotechnol. **8**, 13 (2013).
[3] D.B. Strukov, G.S. Snider, D.R. Stewart, R.S. Williams. Nature letters **453**, 80 (2008).
[4] S.M. Yakout. J. Supercond. Nov. Magn. **34**, *2*, 317 (2021).
[5] N.A. Spaldin, R. Ramesh. Nat. mater. **18**, *3*, 203 (2019).
[6] A.Q. Jiang, C. Wang, K.J. Jin, X.B. Liu, J.F. Scott, Ch.S. Hwang, T.A. Tang, H.B. Lu, G.Z. Yang. Adv. Mater. **23**, 1277 (2011).
[7] Z. Zhao, A. Abdelsamie, R. Guo, S. Shi, J. Zhao, W. Lin, K. Sun, J. Wang, J. Wang, X. Yan, J. Chen. Nano Research **15**, *3*, 2682 (2022).
[8] J. Wu, J. Wang. J. Appl. Phys. **108**, *9*, 094107 (2010).
[9] J. Wu, X. Lou, Y. Wang, J. Wang. Electrochem. Solid-State Lett. **13**, *2*, 9 (2009).
[10] S. Ramazanov, F. Orudzhev, G. Gajiev. Surfaces **7**, *1*, 1 (2024).
[11] S. Ramazanov, F. Orudzhev, G. Gajiev, V. Holcman, R.S. Matos, H.D. da Fonseca Filho, S. Ţălu, D. Selimov. Appl. Surf. Sci. 647, 158863 (2024).
[12] Yu.V. Podgorny, A.N. Antonovich, K.A. Vorotilov & A.S. Sigov. Ferroelectrics **544**, 82 (2019).
[13] Y.V. Podgorny, K.A. Vorotilov, A.S. Sigov. AIP Advances **6**, *9*, 095025 (2016).
[14] Yu.V. Podgorniy, P.P. Lavrov, K.A. Vorotilov, A.S. Sigov. FTT **57**, *3*, 465 (2015). (in Russian).
[15] S. Lancaster, P.D. Lomenzo, M. Engl, B. Xu, T. Mikolajick, U. Schroeder, S. Slesazeck. Front. Nanotechnol. **4**, *17*, 1 (2022).
[16] J.H. Lee, Y. Lee, J.-K. Han, K.D. Kim, S.R. Byun, H.W. Park, C.S. Hwang. Adv. Electron. Mater. **11**, *3*, 2400516 (2024).
[17] G.M. Gadzhiev, Sh.M. Ramazanov, N.S. Abakarova, T.N. Efendieva. FTT **66**, *2*, 259 (2024). (in Russian).
[18] N.P. Bogoroditskiy, Yu.M. Volokobinskiy, A.A. Vorobiev, B.M. Tapeev. Teoriya dielektrikov. Energiya, M.-L. (1965). 344 s. (in Russian).
[19] T. You, N. Du, S. Slesazeck, T. Mikolajick, G. Li, D. Bürger, I. Skorupa, H. Stöcker, B. Abendroth, A. Beyer, K. Volz, O.G. Schmidt, H. Schmidt. ACS Appl. Mater. Interfaces **6**, 19758 (2014).
[20] L.S. Berman, A.A. Lebedev.
[20] Emkostnaya spektroskopiya glubokikh tsentrov v poluprovodnikakh. Nauka, L. (1981). S. 28. (in Russian).
[21] Yu.V. Podgorniy, K.A. Vorotilov, A.S. Sigov. FTT **54**, *3*, 859 (2012). (in Russian).

Translated by M.Verenikina